

Towards multimaterial multifunctional fibres that see, hear, sense and communicate

Virtually all electronic and optoelectronic devices necessitate a challenging assembly of conducting, semiconducting and insulating materials into specific geometries with low-scattering interfaces and microscopic feature dimensions. A variety of wafer-based processing approaches have been developed to address these requirements, which although successful are at the same time inherently restricted by the wafer size, its planar geometry and the complexity associated with sequential high-precision processing steps. In contrast, optical-fibre drawing from a macroscopic preformed rod is simpler and yields extended lengths of uniform fibres. Recently, a new family of fibres composed of conductors, semiconductors and insulators has emerged. These fibres share the basic device attributes of their traditional electronic and optoelectronic counterparts, yet are fabricated using conventional preform-based fibre-processing methods, yielding kilometres of functional fibre devices. Two complementary approaches towards realizing sophisticated functions are explored: on the single-fibre level, the integration of a multiplicity of functional components into one fibre, and on the multiple-fibre level, the assembly of large-scale two- and three-dimensional geometric constructs made of many fibres. When applied together these two approaches pave the way to multifunctional fabric systems.

**A. F. ABOURADDY¹, M. BAYINDIR^{1,4}, G. BENOIT^{2*},
S. D. HART^{2*}, K. KURIKI^{1*}, N. ORF², O. SHAPIRA³,
F. SORIN², B. TEMELKURAN^{1*} AND Y. FINK^{1,2†}**

¹Research Laboratory of Electronics, ²Department of Materials Science and Engineering, ³Department of Electrical Engineering and Computer Science, Massachusetts Institute of Technology, 77 Massachusetts Avenue, Cambridge, Massachusetts 02139, USA; ⁴Department of Physics, Bilkent University, Ankara 06800, Turkey

*Present addresses: 3M Display and Graphics Film Laboratory, 3M Center, Building 0236-02-A-06, St Paul, Minnesota 55144, USA (G. B.); 3M Optical Systems Division, 3M Center, Building 235-1E-54, St Paul, Minnesota 55144, USA (S. D. H.); GE-Plastics, Global Marketing, Global Application Technology, 2-2 Kinugaoka, Moka, Tochigi 321-4392, Japan (K. K.); OmniGuide, One Kendall Square Building 100, 3rd Floor, Cambridge, Massachusetts 02139, USA (B. T.)

†e-mail: yoel@mit.edu

The fabrication and characterization of silica-glass optical fibres^{1,2} have been developed into a precise art by the telecommunications industry³⁻⁶. An unintended side effect of this success has been the focusing of efforts on a small set of materials and structures that provide light guidance in the fibre core through total internal reflection in the transparency range of silica glass. This situation has changed in the last decade. Microstructured fibres have been explored allowing for a larger set of fibre designs, although light guidance still relied

on total internal reflection^{7,8}. Fibres that contain two-dimensional (2D) photonic-crystal structures⁹ that guide light by a photonic bandgap¹⁰⁻¹² (PBG) effect have been demonstrated. The wide variety of results obtained by these fibres has been recently reviewed, and the reader is referred to these reviews for further details^{13,14}. The materials used in these fibres are the traditional materials, namely silica glasses or polymers, with the addition of air holes that may contain fluids¹⁵. The use of electrically insulating materials and the presence of compressible domains restrict applications to optical transmission and associated phenomena.

A few years ago our group posed the question of whether it would be possible to combine a multiplicity of solid materials with disparate electrical, optical and mechanical properties into a single fibre. Could such fibres be realized in arbitrary geometries with low-scattering interfaces between their various material domains? What would determine the lower limit on feature dimensions? And could these fibres be produced through the simple and scalable process of thermal drawing? Doing so would enable a large set of unique and unconventional fibre functions that could be produced at kilometre lengths and low cost, thus defining a new class of optical, electronic, thermal and acoustic devices. In the following sections we attempt to address these questions through the introduction of specific examples of multimaterial fibres each defined by its own unique geometry and composition; all are produced through the simple thermal scaling of a macroscopic multimaterial preform. We begin by establishing the method of

using a multimaterial preform for fibre processing, and outlining the selection criteria for compatible materials combinations.

Next we present a fibre where light is confined to a hollow core by periodically alternating layers of an electrically insulating polymer and a semiconducting glass of prescribed thicknesses, thus forming a cylindrical omnidirectional mirror^{16–20}. The index contrast between layer materials is sufficiently large to minimize the penetration of the electromagnetic field into the solid layers, producing a fibre that is significantly more transparent than its constituent materials. A distinctive feature of this structure is that its properties are wavelength scalable, that is, the period of the structure determines the wavelength of light that is transmitted along the fibre axis. Consequently, the same overall fabrication approach is used to produce fibres that guide ultraviolet (UV), visible, near-infrared (NIR) or mid-infrared (MIR) light by simply changing the lattice constant of the periodic multilayer structure.

The process of drawing long lengths of fibres leads to the generation of large surface area. This in turn presents the opportunity for creating fibre surface devices. By placing the omnidirectional mirror structure close to the fibre circumference, high-efficiency fibre reflectors are obtained on very large areas²¹. Furthermore, inserting specific thickness deviations in particular layers of the reflecting structure leads to the emergence of a radial resonant optical cavity fibre^{22–25}. We next discuss the consequences of co-drawing metals, semiconductors and insulators in the same fibre to produce optoelectronic and thermal fibre-based devices^{23,26–29}. Examples include thin-film²⁷ and solid core^{23,28} metal–semiconductor–metal (MSM) junctions that detect optical or thermal excitation.

These unifunctional building blocks render possible multifunctional fibres that integrate more than one building block into the structure, and fibre arrays where multiple fibres are assembled into large-scale constructs. We review three integrated single-fibre devices: a self-monitoring high-power transmission fibre, a narrow-band photodetecting fibre, and a transverse-emitting fibre laser. Device fibres have been used to construct 2D^{23,28,29} and 3D²⁹ arrays that perform sophisticated optical and thermal imaging tasks. Finally we provide a vision for further developments in this emerging field.

MATERIALS AND PROCESSING

The first step of our method is the fabrication of a multimaterial cylindrical object called a preform, which is identical in its geometry and composition to the final fibre, but is much larger in its cross-sectional dimensions and shorter in length. This preform is thermally drawn into multimaterial ‘composite’ fibres^{20,21,23} consisting of at least two materials having different optical and electrical properties while maintaining the geometry, increasing the length and reducing the cross-sectional dimensions. Key to this process is the identification of materials that can be co-drawn and are capable of maintaining the preform geometry in the fibre and the prevention of axial- and cross-sectional capillary break-up. To achieve this objective, viscous forces are commonly used to oppose the interface-energy-driven capillary break-up mechanisms^{30–34}. The following general conditions are needed in the materials used in this process: (1) At least one of the fibre materials needs to support the draw stress and yet continuously and controllably deform; thus at least one component should be amorphous in nature, and resist devitrification, allowing for fibre drawing at reasonable speeds in a furnace-tower process with self-maintaining structural regularity. Indeed, it is typical that the fibres are drawn under high-stress conditions to counter surface-tension effects. (2) All the materials must flow (viscosity $<10^7$ poise) at a common temperature; if a crystalline material is incorporated it should have a melting temperature below the draw temperature.

(3) The materials should exhibit good adhesion/wetting in the viscous and solid states without cracking even when subjected to rapid thermal cooling.

In structures that are omnidirectionally reflecting, additional restrictions are placed on the materials properties. First, the two materials must have high index-contrast to satisfy the criterion of omnidirectional reflectivity^{17,18}. Second, the materials should exhibit low optical absorption over a common wavelength band (such that the evanescent decay length is shorter than the absorption length).

As glassy materials have a continuous viscosity–temperature dependence and thus lend themselves to high-speed drawing, our materials choices have focused on chalcogenide glasses and polymeric thermoplastics that have a high glass-transition temperature. Chalcogenides are high-index inorganic glasses that contain one or more of the chalcogen elements (sulphur, selenium and tellurium) and generally contain no oxygen. They tend to have glass-transition temperatures in a range between 100–400 °C, refractive indices between 2.2–3.5 (refs 35–40), and are transparent in the infrared. Examples of glass compositions described here include As_2Se_3 , As_2S_3 , $\text{As}_{40}\text{Se}_{50}\text{Te}_{10}\text{Sn}_5$ and $\text{Ge}_{15}\text{As}_{25}\text{Se}_{15}\text{Te}_{45}$.

In selecting a low-index component as the second material for these PBG fibres, it is of principal concern to match the thermal properties of some chalcogenide glass. Although oxide glasses have excellent optical properties, most of them have very high softening temperatures, making them incompatible with chalcogenide glasses in a thermal co-deformation process. Thermoplastic polymers tend to have lower softening temperatures than typical chalcogenide glasses; however, a few candidates have been identified with thermal properties that are in some ways comparable to chalcogenides. Examples of polymers described here include polyether sulphone (PES), polysulphone (PSu) and polyether imide (PEI). Disadvantages of polymeric materials that may need to be addressed include their thermal stability and optical absorption. Nevertheless, the wide variety of polymers available, the feasibility of processing them in film form, and their excellent mechanical toughness makes these materials principal candidates for combination with chalcogenide glasses in composite PBG fibres.

In producing optoelectronic fibre devices metals need to be co-drawn along with the glasses and polymers. As the metallic elements should have a melting temperature below the drawing temperature, only low-melting-point metals or alloys are suitable for the thermal-drawing process. Several metals have been incorporated into fibre devices thus far, such as Sn, In, Bi and eutectics of Au, Bi and Sn.

BASIC UNIFUNCTIONAL FIBRE STRUCTURES

CYLINDRICAL HOLLOW PBG TRANSMISSION FIBRES

The transmission of electromagnetic waves in hollow waveguides dates back to Southworth and his seminal work on metallic-waveguide modes in the 1930s⁴¹. In the early 1970s, Bell Labs deployed the WT4 long-haul communication system^{42,43} designed to transmit millimetre waves in a hollow metallic tube. The advent of high-purity silica fibres set the basis for modern optical communications, where light is guided by total internal reflection in solid materials, a process that has fundamental limitations stemming from light absorption by electrons and phonons, material dispersion, Rayleigh scattering and various nonlinear effects⁴⁴. These limitations have motivated the study of light propagation in hollow fibres with many applications in high-power laser guidance for medical procedures⁴⁵, atom guiding⁴⁶, high-harmonic generation^{47,48}, among others. Hollow-fibre technology is not without precedent, and hollow metallic or metallo–dielectric waveguides have been studied extensively and have found use

Box 1 Fibre fabrication

To give an outline of the steps involved in fibre fabrication, we consider an integrated device (Fig. 5) that consists of both a cylindrical omnidirectional mirror structure and a metal–semiconductor–insulator optoelectronic device.

Fabricating the device fibre begins with synthesizing a chalcogenide glass rod using standard sealed-ampoule techniques^{35,38,39}. A hollow polymer tube is prepared having an inner diameter that exactly matches the outer diameter of the glass rod, and a thickness exactly equal to that of thin metallic ribbons. The glass rod is then slid into the tube, the electrodes are inserted into pockets cut in the tube (Fig. B1a), and finally a protective polymer cladding is wrapped around the structure (Fig. B1b). In this way, the metal electrodes are completely enclosed between the polymer and the glass rod, preventing any leakage when it melts during drawing. The electrodes may be also contacted to thin glass films with this method (F. Sorin *et al.*, manuscript in preparation).

Fabrication of hollow multilayer structures in fibres begin by thermally evaporating a high-index chalcogenide glass on both sides of a free-standing low-index thin polymer film. To create a

hollow fibre, the film is wrapped around a silicate glass tube and consolidated through heating in a vacuum oven. The silicate tube is then removed from the preform core by etching with hydrofluoric acid. When the structure is placed on the external surface of the fibre, no quartz tube is needed. Instead, the coated film is rolled directly around a polymer cylinder with a thin protective polymer layer wrapped around it.

Both procedures are combined in preparing the preform shown in Fig. B1, where an external multilayer structure surrounds the optoelectronic device. The preform is then consolidated under vacuum at a high temperature (typically 10^{-3} torr and 260 °C). The resulting fibre preform is thermally drawn into extended lengths of fibre using the tower draw procedure common in the fibre-optic industry. During the draw process, the mirror layers are reduced in thickness by a factor of approximately 20–100 and the nominal positions of the PBGs are determined by laser micrometre monitoring of the fibre outer diameter during the draw process. The end result of this fabrication process is hundreds of metres of uniform fibres.

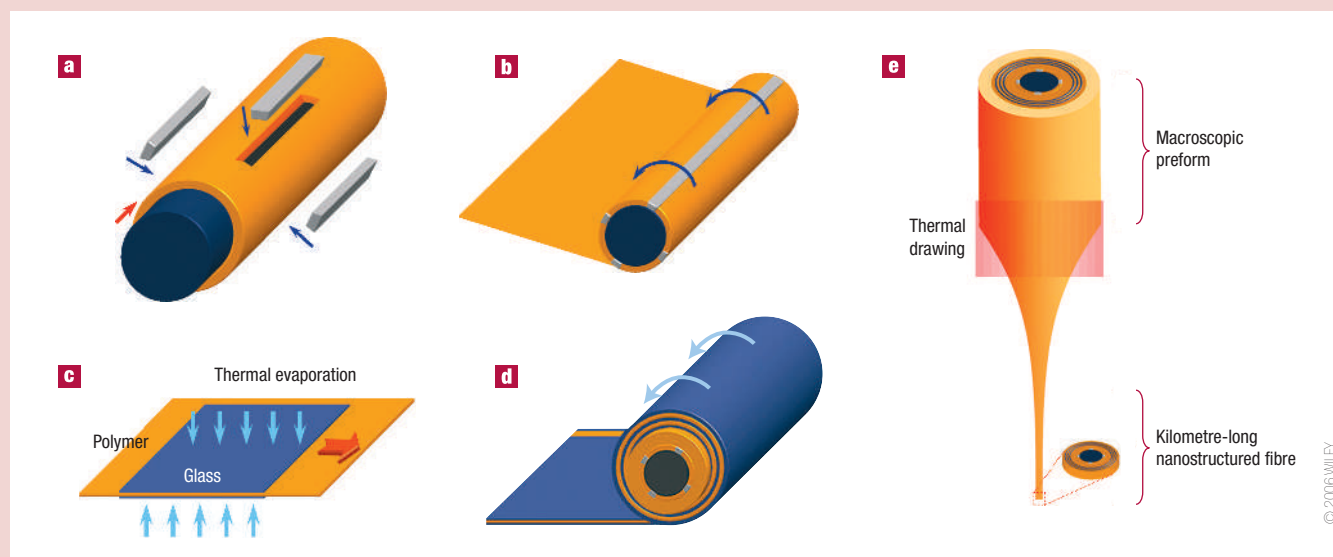


Figure B1 Preform-based fabrication of integrated fibre devices. **a**, A chalcogenide semiconducting glass rod is assembled with an insulating polymer shell and four metal electrodes; and **b**, a polymer sheet is rolled around the structure to form a protective cladding. **c**, The high-index chalcogenide glass is evaporated on both sides of a low-index thin polymer film before **d**, being rolled around the cylinder prepared in **a,b**. A polymer layer is wrapped around the coated film for protection. **e**, The preform is consolidated in a vacuum oven and is thermally drawn to mesoscopic-scale fibres. The cross-section of the resulting fibres retains the same structure and relative sizes of the components at the preform level. Reprinted with permission from ref. 28.

in several practical applications^{49,50}. Nevertheless, finite metal conductivity in the visible and NIR results in high transmission losses, and the process used to deposit metallic linings limits the fabrication length of these fibres and their flexibility.

Exploration of Bragg reflection as a mechanism for light guidance in a hollow core was initiated in 1978 by Yariv and colleagues¹⁶, and later by Miyagi and Nishada⁵¹, who theoretically investigated the transmission of non-index-guided modes through a hollow multilayer cylindrical structure by Bragg reflection from the cladding. Nevertheless, limitations on the index-of-refraction

contrast inherent in doped-silica technology led to pessimistic assessments of the potential of this approach⁵². However, using the above described materials and processing approach, hollow-core optical fibres with an interior omnidirectional dielectric mirror may be produced (see Boxes 1 and 2, and Fig. 1a,b). Confinement of light in the hollow core is provided by the large PBGs established by the multiple alternating layers of a high-refractive-index glass and a low-refractive-index polymer. The same polymer may be used as a protective cladding material, resulting in fibres composed of 98% polymer by volume (not including the hollow core); the fibres thus

Box 2 Omnidirectional reflection and light guidance

Although metallic mirror reflectors have been known for a long time and are attractive because they reflect light over a wide angular range, their usage in optics has been limited because of high optical losses. Multilayer interference filters, on the other hand, have low optical losses but exhibit high reflection over a limited angular range. It was recently recognized that a finite 1D periodic structure (Fig. B2a) can be designed that combines the advantages of both while avoiding the drawbacks: a mirror with low-loss omnidirectional reflectivity. In order to achieve this, conditions must be met on the refractive index contrast n_H/n_L (where n_H and n_L are the refractive indices of the layers) and on the ratio of the lower index to the ambient n_L/n_A ($n_A = 1$ here) leading to a photonic band diagram such as that shown in Fig. B2b. There propagating Bloch states are shown in brown whereas forbidden states are in white on a frequency ω versus wave vector β diagram for both polarizations (TE and TM). Light incident from an ambient medium is limited to that portion of the figure that is above the light lines ($\beta = \omega/c$). Externally incident light in the range of frequencies shown in grey cannot couple to any propagating states within the structure and will be reflected regardless of the angle of incidence (0° or $\beta = 0$ to 90° or $\beta = \omega/c$) or polarization.

This omnidirectional reflector may then line the interior of a hollow-core cylindrical fibre to guide light along the axis¹⁹ (Fig. B2c). In a finite cylindrical structure the translation symmetry in the direction parallel to the layers is preserved and the plane waves are replaced by cylindrical waves in the form of Bessel functions⁸⁰. The relevance of the band diagram here is that we expect the light to be confined to the core in a frequency range that corresponds to the bandgap of a planar structure having the same structural parameters. The boundary conditions imposed by the structure allow for the existence of discrete propagating modes inside the bandgap (brown lines in Fig. B2d). The vector field distributions of three modes of particular interest (HE_{11} , TE_{01} and TM_{01})^{81,82} are shown in the inset of Fig. B2d.

Although premonitions of this fibre transmission mechanism have existed since the 1970s¹⁶, this structure was not vigorously pursued for two primary reasons: (1) the periodicity of the multilayers must be a fraction of a wavelength maintained over extended lengths of fibre, and (2) the high-index contrast needed between the layers usually entails very different thermo-mechanical properties, thus excluding traditional thermal drawing as a fabrication approach. The work outlined in this review aims at showing that such a fibre is in fact feasible even with these seemingly daunting difficulties.

combine high optical performance with polymeric processability and mechanical flexibility, as seen in Fig. 1a.

The ‘wavelength scalability’ of these hollow-core fibres (that is, the control of spectral transmission through the fibre’s structural parameters) is demonstrated by producing fibres in an identical fashion with transmission peaks in the UV, visible, NIR⁵³ and the MIR²⁰ regions of the optical spectrum. Scanning electron microscope (SEM) imaging of the layers (Fig. 1c,d) reveals that the final layer thicknesses correctly correlate to the measured transmission peaks (Fig. 1e). Hollow-core cylindrical PBG fibres have been produced with fundamental PBGs at 350 nm (UV), at 750 nm (NIR) for biomedical applications, at 1.5 μm (NIR) for use in telecommunications applications, at 2.94 μm (MIR) for the transmission of high-energy Er:YAG laser radiation (not shown in Fig. 1e), and at 10.6 μm (MIR) for laser surgery and materials processing.

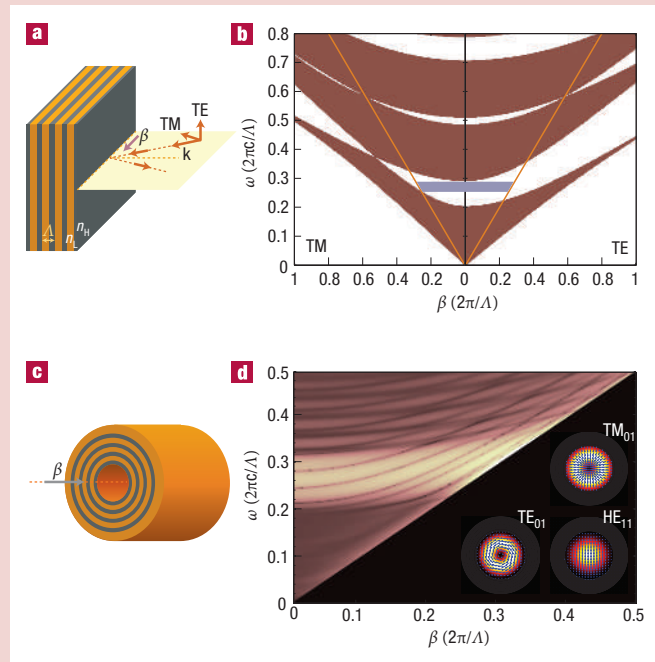


Figure B2 Omnidirectional reflection and light guidance. **a**, A 1D planar dielectric multilayer structure composed of alternating layers of indices n_L and n_H ($n_H > n_L$) of period Λ ; β is the component of the wave vector k parallel to the structure. The direction of the electric field vectors for the transverse electric (TE) and transverse magnetic (TM) modes are shown. **b**, The TE and TM band diagram of the structure in **a**. The two orange lines are the light lines in the ambient medium ($\omega/\beta = c$, assuming the surrounding medium has $n = 1$). Propagating Bloch states are shown in brown whereas forbidden states are in white. **c**, A hollow-core fibre lined with a cylindrical omnidirectional reflecting structure guides light along the axis (β is the axial wave number). **d**, The band diagram for the fibre in **c**, where dark brown corresponds to allowed photonic states and white corresponds to forbidden states. Similar parameters to those for the structure in **a** were used, and the location of the PBG is similar to that in **b** for the planar structure. Note that allowed modes are now introduced into the PBG. The inset shows the vector field distribution of three low-order modes: TE_{01} , TM_{01} (both having angular momentum 0), and HE_{11} (hybrid mode, having angular momentum 1).

One reasonable figure-of-merit for optical transmission losses through hollow all-dielectric PBG fibres is a comparison of the hollow fibre losses to the intrinsic losses of the materials used to make the fibre²⁰. Reported losses at 10.6 μm for commercially available As_2Se_3 are typically of the order of 10 dB m^{-1} , whereas optical losses for PES exceed 30,000 dB m^{-1} . Transmission losses at 10.6 μm in hollow-core PBG fibres fabricated out of these two materials are typically lower than 1 dB m^{-1} , demonstrating that the waveguide losses are orders of magnitude lower than the intrinsic fibre material losses. This is made possible by the short penetration depths of electromagnetic waves in the high-refractive-index-contrast photonic-crystal structure, allowing these materials to be used at wavelengths that have so far been thought improbable.

Another long-standing motivation of infrared-fibre research has been the transmission of high-power laser light⁵⁰. Although

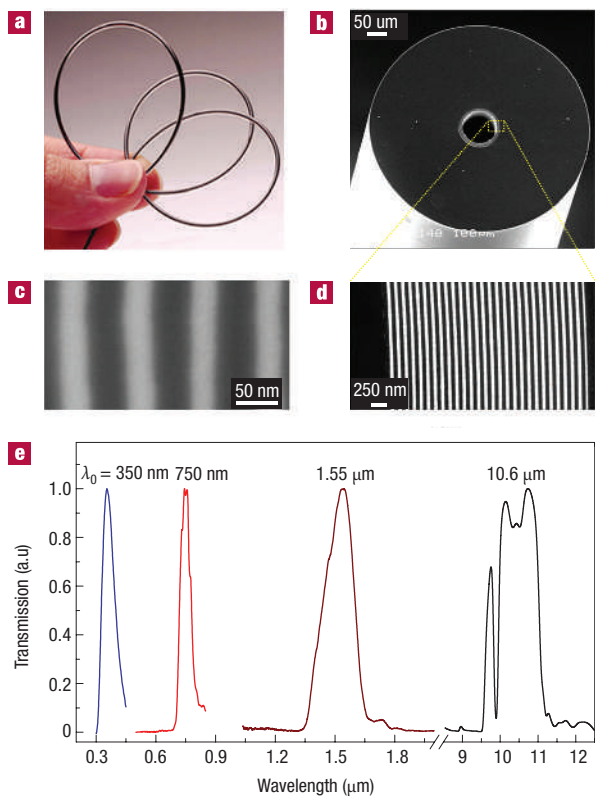


Figure 1 Wavelength-scalable hollow-core PBG fibres. **a**, A flexible, hollow-core, PBG fibre. **b**, A scanning electron microscope (SEM) micrograph of a hollow-core PBG fibre cross-section. **c,d**, SEM micrographs of the omnidirectional reflecting multilayer structures lining the hollow fibre core for UV (**c**) and NIR (**d**) transmission peaks. **e**, Wavelength scalability of hollow-core PBG fibres. Transmission spectra of four fibres, differing only in the period of the multilayer structure, with peak wavelengths λ_0 at 10.6 μm , 1.55 μm (corresponding to the structure in **d**), 750 nm, and 350 nm (corresponding to the structure in **c**).

powerful and efficient CO_2 lasers at 10.6 μm are available, waveguides operating at this wavelength have remained limited in length and have high loss levels^{54,55}. The transmission of CO_2 laser light with power densities exceeding 1.3 kW cm^{-2} (25 W in a 500 μm hollow-core diameter) has been demonstrated, a power density sufficient to burn holes in a film of PES (the fibre majority component). CO_2 lasers have been traditionally used for non-invasive upper airway surgery due to excellent laser-tissue interactions^{56,57}. Radiation at 10.6 μm delivers precise incisions at high-power densities while providing haemostatic properties at lower power densities. The absence of a flexible fibre limited surgeons to treatment of lesions above the vocal chords where line-of-sight techniques could be used. The advent of flexible CO_2 -laser-transmitting fibres enables surgeons to gain access to otherwise inaccessible areas^{58–61} such as the trachea, nasal canals, and even into the bronchi.

CYLINDRICAL OPTICAL RESONATORS

Lining a hollow-fibre core with an omnidirectional reflector confines light and guides it along the fibre axis. However, placing the reflector on the outer surface of the fibre will reflect light impinging on it externally with high efficiency²¹. The fibre structure shown in Fig. 2a, where an optical cavity defect is inserted into an exterior multilayer dielectric omnidirectional reflector^{22,24}, leads to a polymer fibre that is at the same time a high-efficiency

omnidirectional reflecting mirror. These fibres may be incorporated into woven fabrics for precise spectral-identity verification or as radiation barriers, and may also be used as cost-effective tunable optical filters.

The usefulness of this design has been further highlighted by producing cavity resonators in the external 1D photonic crystal, resulting in resonant tunnelling at a frequency inside the PBG (Fig. 2a,b). Moreover, this resonant wavelength may be tuned dynamically. Using mechanical tuning, by applying an axial stress to the fibre ends in the elastic regime, the applied strain leads to a linear shift of the Fabry–Perot resonant mode within the bandgap²². An alternative approach to tuning the Fabry–Perot resonance is through optical modulation of the cavity material properties to obtain an all-optical tunable microcavity fibre²⁴. Here the cavity material is chosen such that it exhibits a transient photodarkening effect, for example As_2S_3 and As_2Se_3 . Photodarkening is an illumination-induced red shift of the optical absorption edge commensurate with an increase of the real part of the refractive index, as dictated by the Kramers–Kronig relations⁶². Part of this effect is fully reversible at room temperature (called transient photodarkening, ref. 63) and may be induced by illumination with the 514-nm line from an argon laser (green arrow in Fig. 2c), resulting in a shift of the resonant wavelength.

Tight control of the spectral behaviour of the fibres is demonstrated in Fig. 2d, where two arrays of fibres with different PBGs are shown. The colours of the fibres shown here correspond to higher-order bandgaps with possible application as an optical barcode for fabric identification.

METAL–SEMICONDUCTOR–INSULATOR DEVICE FIBRES

The combination of conductors, semiconductors and insulators in well-defined geometries and prescribed sizes is essential to the realization of functional electronic and optoelectronic devices. These devices are typically produced using a variety of elaborate wafer-based processes, which afford small features, but are restricted to planar geometries and limited coverage area. This fabrication approach has been the cornerstone of the electronic revolution but has had no impact on the optical-fibre industry, which relies on a very different fabrication technique. We describe here the production of fibres that deliver electronic and optoelectronic functionalities maintained uniformly over extended lengths of a fibre using the preform-based fibre-drawing technique (see Box 1).

A large-scale macroscopic version of the device is prepared in a cylindrical preform, which is then reduced to the desired size through the process of thermal drawing²⁶ (Box 1). The result is kilometre-long functional mesoscopic-scale device fibres, cross sections of which are shown in Fig. 3a,b. In fact, it is conceivable that all the basic components of modern electronic and optoelectronic devices (such as junctions, transistors and so on) could potentially be incorporated into fibres produced with this simple and yet low-cost technique on a length scale beyond the reach of traditional electronics.

When light impinges externally on the (amorphous) semiconductor in the fibre core, free charge carriers are generated. The metal electrodes (which interface with the core along the fibre length) are connected to an external circuit (Fig. 3c). The fibre undergoes a change in electrical conductivity when externally illuminated, as shown by the change in slope of the current–voltage curve on illumination with respect to dark conditions (Fig. 3d). Substituting the bulk semiconducting glass core (Fig. 3a) with a thin-film glass layer (Fig. 3b) leads to an increase in photosensitivity (by almost two orders of magnitude) by eliminating the dark current produced by the volume of the core to which light does not penetrate (F. Sorin *et al.*, manuscript in preparation), and further suggests wider possibilities for fibres

with multiple functionalities achieved by combining several thin-film devices in the same fibre.

The uniqueness of this new type of light-sensing device (besides its low cost and simplicity of production) resides in its geometry. It is the first 1D photodetector that detects light incident on it from any direction at any point along its entire length, which may extend to hundred of metres. A photodetecting line consisting of point photodetectors (of dimensionality 0) would require a large number of devices, and the price of their assembly scales with the detection length required. An inherent disadvantage of an integrating 1D photodetector such as this fibre is that no information about the location of the incident beam along the fibre is obtained. This may be overcome, however, by constructing 2D assemblies of fibres to localize a point of illumination in a plane (see later).

Note that changing the chemical composition of the glass core can change the spectral characteristics of the photoconductive response. In fact, the photoconductive glass may be substituted with other families of glasses that are sensitive to other physical quantities, such as temperature or chemical contaminants. Figure 3e shows the temperature dependence of the resistance of a fibre with similar cross-section to that shown in Fig. 3a, but with the core made of a thermally sensitive glass. The same behaviour is observed when these glasses are incorporated into the fibre in the form of a thin film (Fig. 4). Arrays of these fibres may be used to produce thermal images over large length scales (see later).

INTEGRATED FIBRES

We have thus far described several structural elements (cylindrical multilayers, radial Fabry–Perot cavities, metal–semiconductor–metal junctions) that were realized within single fibres, resulting in unifunctional fibre devices for hollow-core transmission, external reflection and photodetection. However, it is possible to incorporate a multiplicity of such structures into a single fibre, resulting in integrated fibre devices. In this section we discuss three examples of such integration, although a much wider range of applications may be envisioned: (1) a self-monitoring high-power optical transmission line; (2) a narrow-band 1D photodetecting fibre; and (3) a transverse surface-emitting fibre laser.

SELF-MONITORING OPTICAL FIBRES

Hollow-core PBG fibres are potentially important for transmitting high optical power with applications in industrial and medical fields. As the power carried in such fibres increases, the potential adverse effects of inadvertent release of this energy increase accordingly. Thus predicting imminent failure is advantageous.

A fibre that is capable of sensing imminent failure is achieved using the structure shown in Fig. 4a, where a hollow-core PBG transmission fibre (Fig. 1), designed to transmit a high-power CO₂ laser beam, is combined with a thin-film heat-sensing metal–semiconductor–insulator device²⁷ (Fig. 3b) whose conductivity increases with increase in temperature. As the fibre conductivity depends exponentially on the peak temperature along its length, the different types of energy dissipation mechanisms may be distinguished, even when the amount of energy dissipated remains fixed. Figure 4b shows a thermal infrared image of a fibre section where a point defect was intentionally burnt into the fibre while the laser beam propagated through the fibre. The energy released at the localized defect raises the temperature of the fibre significantly in the vicinity of the defect (as detected by the camera), decreases the resistance of the semiconductor layer and produces a large current in the MSM device (circle in Fig. 4c). When the same energy is dissipated in a straight defect-free fibre of same length, the peak temperature along the fibre is lower, and the measured current is also lower (triangle in Fig. 4c). When the fibre was bent (bend

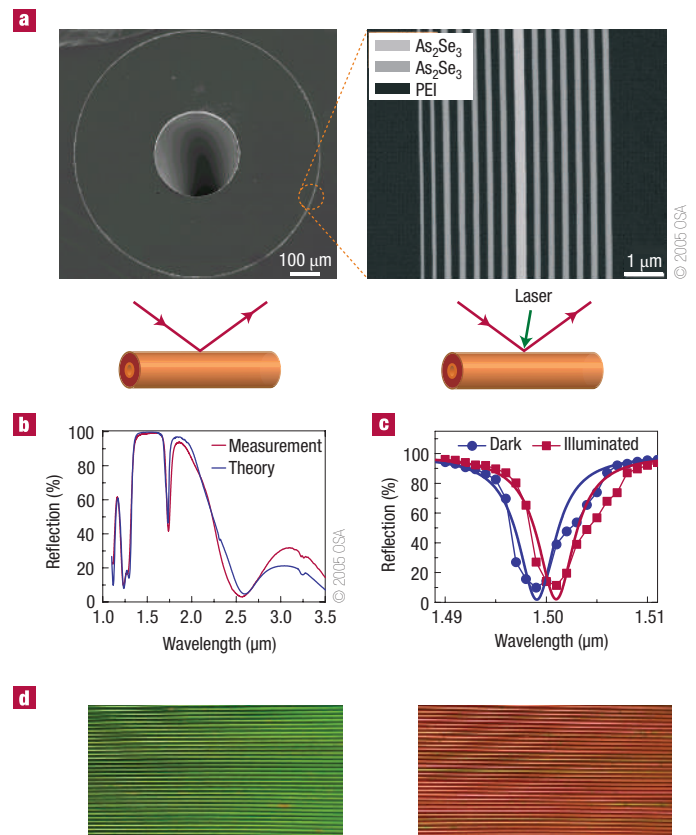


Figure 2 Tunable external reflection microcavity PBG fibres. **a**, SEM micrographs with increasing magnification of the cross-section of a fibre enveloped with an omnidirectional multilayer structure that includes an optical cavity defect layer. **b**, External reflectivity spectrum of a fibre with a low-index defect cavity showing the cavity resonance within the reflection bandgap. Parts **a** and **b** reprinted from ref. 24. **c**, Optical tuning of the cavity resonance for a high-index-cavity using the photodarkening effect. A sub-band laser (green) is used to change the index of the cavity (through the photodarkening effect). As a result, the resonance wavelength at the probe wavelength (red) is shifted. We measured a reversible photo-induced shift of the cavity resonant mode at room temperature of a 910- μm diameter fibre of 2 nm under 574 mW cm⁻² illumination, corresponding to a maximum change in reflectivity of 58% at 1,497.5 nm (ref. 24). **d**, Photographs of external reflecting fibres having different bandgap position. The diameter of the fibres is approximately 500 μm .

radius 10 cm) and the same power dissipated, a peak temperature and measured current (square in Fig. 4c) that are intermediate between the defect-free and localized-defect cases were measured. This makes possible the placement of a threshold (I_c in Fig. 4c) for safe operation of the fibre — exceeding this threshold is a precursor to failure.

NARROW-BAND PHOTODETECTORS

As the spectral range of photodetection of amorphous chalcogenide glasses is typically very wide, they are not useful as narrow-band photodetectors. Nevertheless, by combining the 1D photodetecting fibres with external omnidirectional reflecting structures, the penetration of a very narrow band of wavelengths to the photoconductive core can be engineered, resulting in a 1D narrow-band photodetector²³. This is done by placing a microcavity in the mirror structure to allow the desired wavelength (and desired

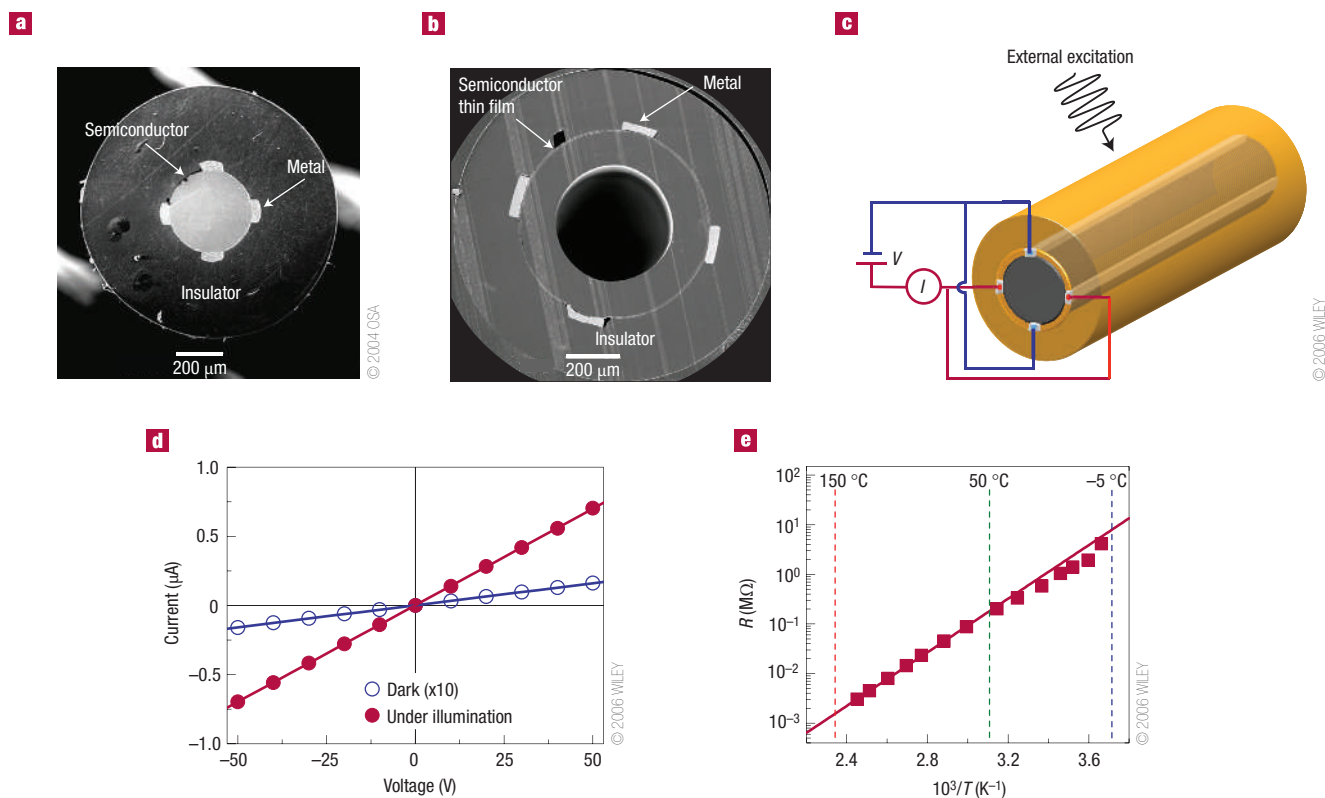


Figure 3 Metal–semiconductor–insulator fibre devices. **a**, SEM micrograph of a cross-section (the semiconductor is $\text{As}_{40}\text{Se}_{50}\text{Te}_{10}\text{Sn}_5$, the insulator polymer is PES, and the metal is Sn). Image reprinted from ref. 26. **b**, SEM micrograph of a thin-film fibre device (the semiconductor is As_2Se_3 , the insulator polymer is PES, and the metal is Sn). **c**, Electrical connection of the four metal electrodes at the periphery of the fibre to an external electrical circuit. **d**, The current–voltage characteristic curve of a photosensitive solid-core fibre device (980 μm outer diameter, 15 cm long). The conductivity increases upon illumination (20 mW, white light) when compared with dark conditions. **e**, The resistance of a thermally sensitive solid-core fibre device (1,150 μm outer diameter, 9 cm long) as a function of temperature. **c–e** reprinted with permission from ref. 28.

bandwidth) to traverse the structure while reflecting all other wavelengths. Figure 5a shows this integrated fibre device highlighting the different structures included in it. We measured both the external reflectivity of the fibre (Fig. 5b) and the fibre photocurrent (Fig. 5c) while scanning the incident wavelength. The functionality of this integrated device is found to be correctly correlated with the structure as shown by the shift of the resonant cavity defect wavelength with change in outer diameter of the device.

SURFACE-EMITTING FIBRE LASERS

All fibre lasers produced to date emit light along the fibre axis with a spot size dictated by the core radius and a nearly planar wave front. Reflection from the end facets of the fibre provides the cavity required for lasing. There are many applications where it is beneficial to deliver laser light in the radial direction over an extended area, such as medical applications ranging from photodynamic therapy⁴⁵ to *in vivo* molecular imaging⁶⁴, as well as textile fabric displays⁶⁵.

Omnidirectional reflection from a multilayer annular mirror lining a hollow-core fibre results in a radial lasing configuration²⁵. The natural curvature of the PBG edges towards higher frequencies with increase in wave number (see Box 2, Fig. B2b) enables simultaneous optical confinement of two frequencies at distinct wave numbers. An optically pumped gain medium is inserted in the fibre core (in this specific case a fluorescent organic dye incorporated into a copolymer matrix) such that the emission spectrum of the

medium lies within the omnidirectional bandgap at $\beta = 0$ (normal incidence to the structure). The higher-frequency optical pump is guided along the fibre axis (high wave number), whereas the lower-frequency laser emission is confined in the transverse direction (low wave number) as shown schematically in Fig. 6a. This results in laser emission in the radial direction from the fibre surface at the location corresponding to the placement of the gain medium as shown in Fig. 6b.

The laser light emitted by this fibre laser has several unique features. The beam is emitted in the radial direction from an extended surface area. The optical wave front is azimuthally anisotropic having a dipole-like radiation pattern for a linearly polarized pump (Fig. 6c). Furthermore, the direction of laser emission is determined by the pump polarization: rotating the linear pump polarization results in rotating the emission direction. Lasers with emission lines throughout the visible and NIR (Fig. 6d) may be constructed using a variety of dyes and scaling of the fibre bandgaps.

FABRIC AND FIBRE WEB SYSTEMS

In the previous section we explored some examples of integrating multiple structures into a single fibre to attain more sophisticated functionality. Another geometric degree of freedom is available through the incorporation of more than one fibre into large-area arrays that introduce functionalities not inherent in the single fibres.

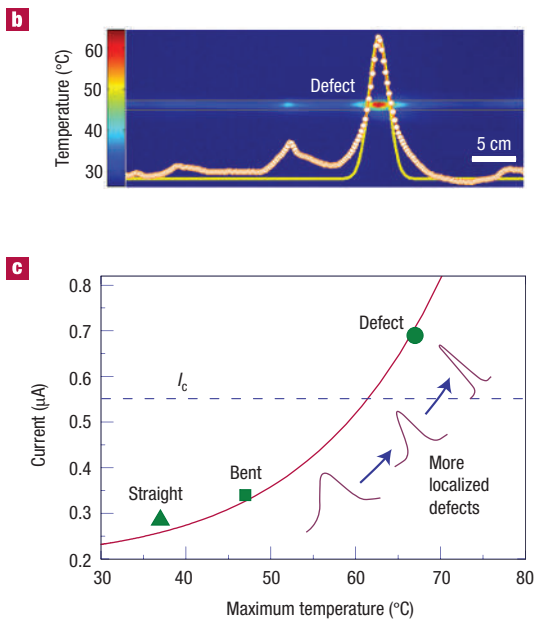
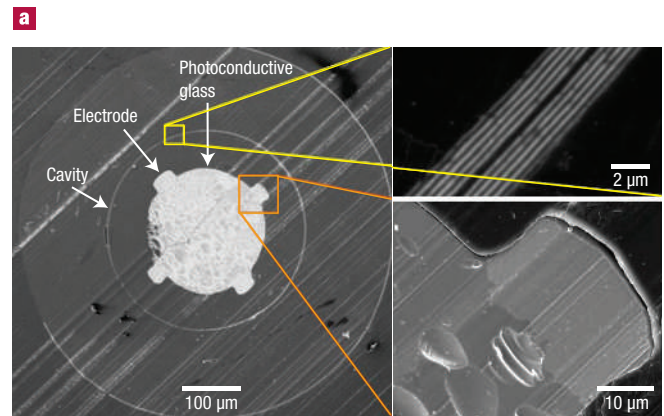
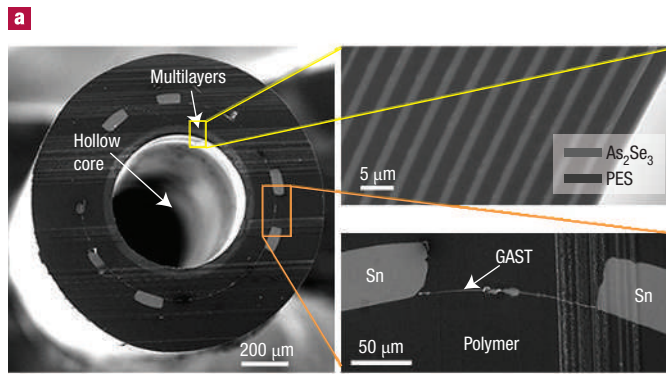


Figure 4 Self-monitoring hollow-core fibres. **a**, SEM micrograph of a self-monitoring-fibre cross-section highlighting the different structures integrated into the device. The inset on the lower right shows the thermally sensitive MSM junction (see Fig. 3b). GAST is gallium–arsenide–selenium–telluride. The upper right inset shows the multilayer structure lining the hollow core designed to guide a high-power CO₂ laser at 10.6 µm (see Fig. 1). **b**, A thermal image of a fibre transmitting a CO₂ laser beam. A defect was intentionally created in the fibre at the location of the peak in the measured temperature profile (fitted to a gaussian profile). **c**, Measurement of the MSM fibre device current at fixed dissipated power for three fibres: straight (triangle), bent (square), and straight fibre containing a defect (circle) as shown in **b**. Figures reprinted from ref. 27.

For example, although a single photosensitive (or thermally sensitive) fibre cannot determine the location of a point of excitation along its length, arranging a multiplicity of identical fibres over a grid enables a point of optical (or thermal) excitation to be localized over the area of the grid. The detection of a point of optical or thermal excitation on an $N \times N$ grid normally requires the order of N^2 point detectors, but an array of linear 1D detectors produces the same capability with the order of N detectors only^{23,26} (compare to traditional optical and thermal imaging systems described in, for example, refs 66,67).

An example of such an array is shown in Fig. 7a, where thermally sensitive fibres (having the structure shown in Fig. 3a) are woven

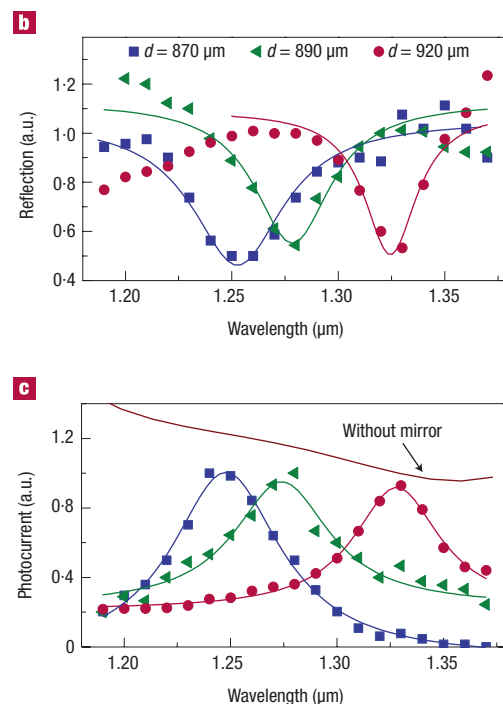


Figure 5 Narrow-band photodetecting fibres. **a**, SEM micrograph of a narrow-band photodetecting fibre cross-section highlighting the different structures integrated into the device. The inset on the lower right shows the metal–semiconductor interface (see Fig. 3a) and the upper right inset shows the external multilayer structure containing a low-index cavity (see Fig. 2a). **b**, Measured external reflectivity of three fibres with different outer diameters showing that the location of the resonance wavelength shifts proportionally to the diameter. **c**, The photocurrent for the fibres in **b** is measured simultaneously with the reflectivity showing that the peak photocurrent occurs at the resonance wavelengths. The photocurrent of a fibre without a mirror surrounding it is also shown. Figure reprinted from ref. 23.

into a fabric placed on a curved surface to form an 8×8 array with 1-cm spacing²⁸. Several unique features of the fibres are brought out in this example. They are flexible and lightweight, and may thus be incorporated into pre-existing structures. Furthermore, as the fibres are produced uniformly in long lengths, the arrays built out of them may extend over large areas.

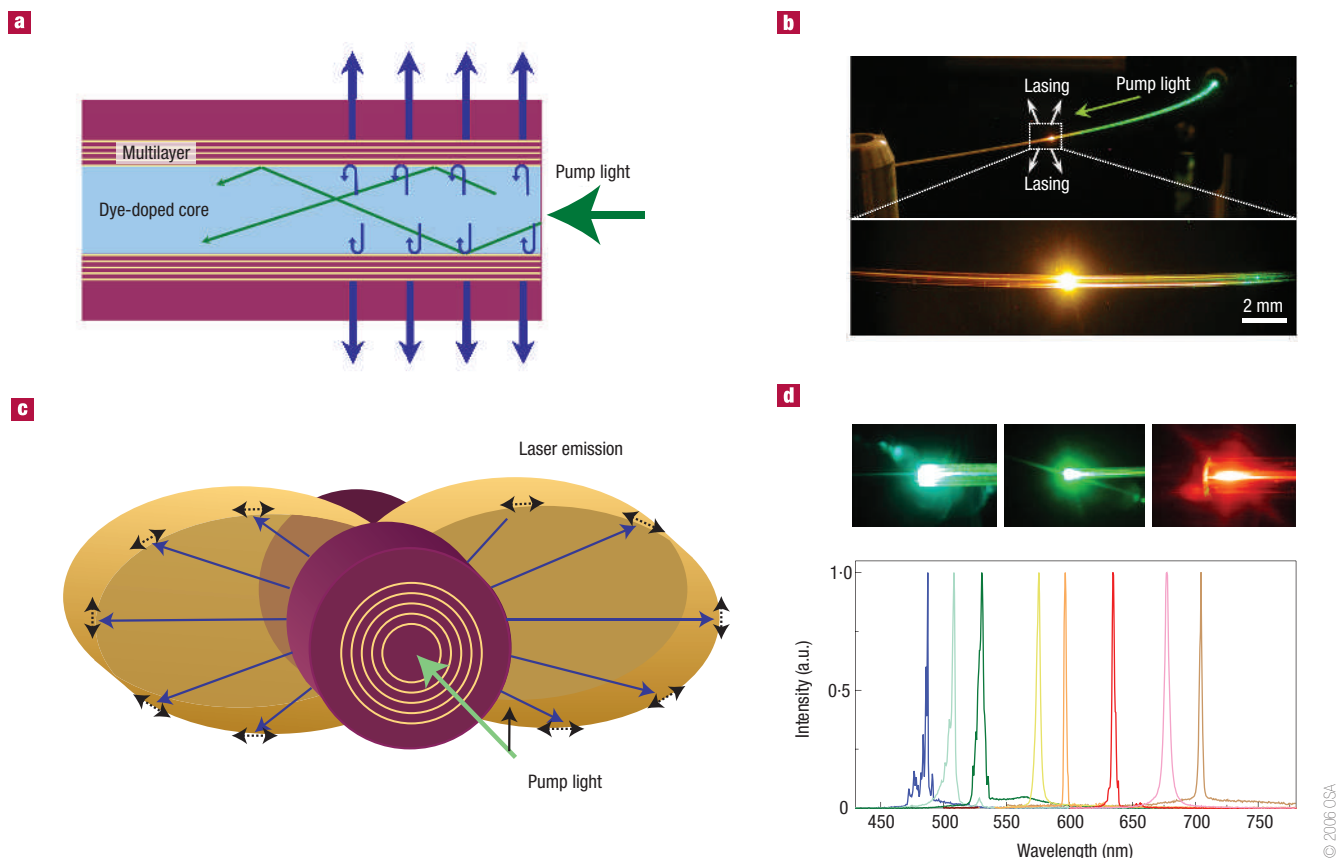


Figure 6 Surface-emitting fibre lasers. **a**, Schematic illustrating the operating principle of the surface-emitting fibre laser. A gain medium is inserted into the hollow core of a transmission PBG fibre. An optical pump is guided along the fibre exciting the dye molecules. The fluorescence is emitted at a longer wavelength and the fibre laser emits light in the transverse direction. **b**, A demonstration of the dual role of the hollow-core PBG fibre: the pump (532 nm, green) is guided in the hollow-core PBG fibre and lasing (576 nm, orange) occurs in the dye-doped region. **c**, Geometric dependence of the emission for a PBG fibre laser. Angular intensity pattern of the bulk dye and fibre laser emission at a fixed location along the fibre axis as measured by rotating the input polarization. This measurement is equivalent to fixing the pump polarization while measuring the emission intensity around the fibre. **d**, Laser emission spectra from fibres doped with nine different dyes showing the wavelength scalability of our fibre lasers. The inset shows photographs of the organic dye-doped PBG fibre lasers showing the individual laser colours (blue, green and red) emitted from the fibre surface. Figures reprinted with permission from ref. 25.

As the fibre webs are essentially transparent, new topologies can be explored that enable the determination of the direction of excitation in addition to the location²⁹. The closed spherical detector shown in Fig. 7b consists of photosensitive fibres (Fig. 3a) arranged on the sphere's latitudes and longitudes. A ray of white light traverses the structure intersecting with it twice, allowing us to reconstruct the path of the ray from the reconstruction of the fibre photoconductivity over the curved spherical surface.

More sophisticated optical processing tasks also may be achieved using 2D and 3D fibre webs. In particular, we have demonstrated that a 2D fibre web may be used to reconstruct an arbitrary optical intensity distribution through the use of a tomographic reconstruction algorithm²⁹. The phase-retrieval algorithm may be used to reconstruct both the amplitude and phase of an optical wave front passing through two planar fibre arrays²⁹. Thus moving from 2D to 3D structures paves the way to full optical and thermal imaging capabilities to be realized²⁹.

Finally, in Fig. 7c we show an example of both levels of integration applied simultaneously: integrating multiple structures into a single fibre, and integrating multiple fibres into an array. The fabric shown is a 2D fibre web woven out of narrow-band

photodetecting fibre devices as previously described (Fig. 5). Each fibre detects light of a certain colour along its whole length. The fibres have fundamental PBGs in the visible spectrum with resonant cavities that allow for only a narrow spectral band to penetrate to the semiconducting glass core. Electrical signals collected at the periphery of the fibres in the arrays map out a spectral image. The small average diameter of the fibres makes them more flexible, enabling a tightly woven fabric²³.

FUTURE DIRECTION AND VISION

We expect future research to focus on a number of key areas: identification of new materials; the improvement of the quality of materials and interfaces; new fibre-device architectures; and the increase of device density through the reduction of feature sizes. Many polymer materials are potentially compatible with this processing approach, ranging from piezoelectric polymers for the purpose of fibre acoustic transduction to conjugated polymers for light emission. Although we have to date relied on inorganic chalcogenide glasses for optoelectronic functionality and ease of processing, it is expected that by inducing phase transitions^{68–70}

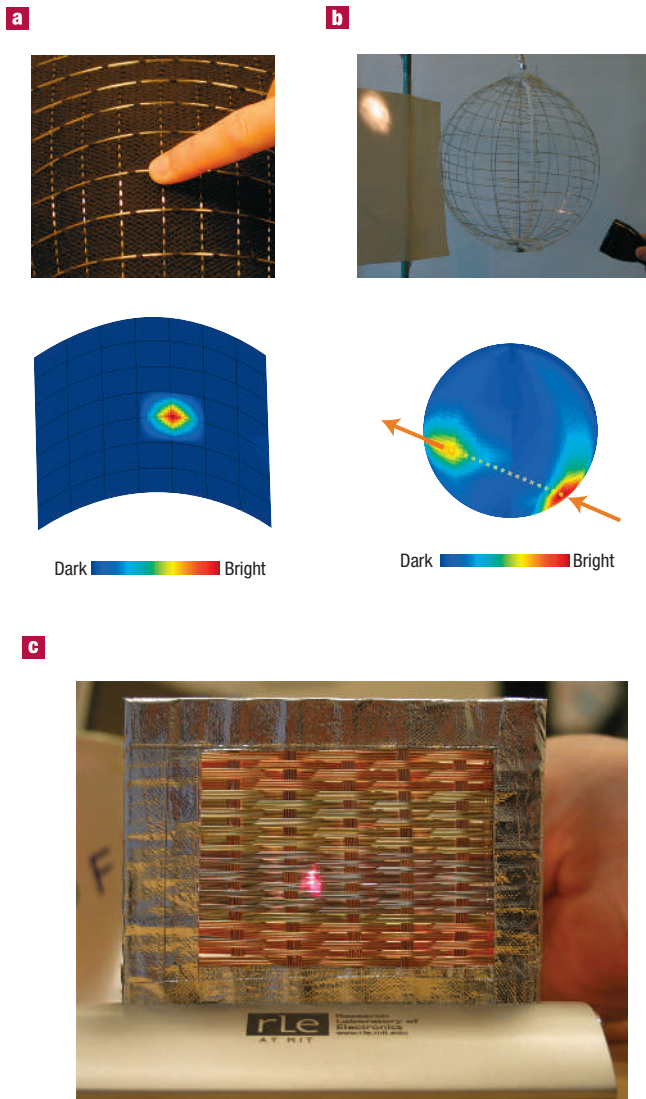


Figure 7 Two- and three-dimensional optical and thermal fibre arrays. **a**, A 2D array of thermally sensitive fibres (8×8 with 1-cm separations) woven into a fabric on a curved surface. The lower panel shows a reconstruction of the thermal distribution on the fabric after the touch of a finger. The reconstruction was done using electrical-current measurements obtained from the fibres after the finger was removed, and the data is plotted on a curved surface for clarity. Image reprinted with permission from ref. 28. **b**, A closed 3D spherical array constructed of optically sensitive fibres detects the direction of a ray of light. The fibres are arranged over the latitudes and longitudes of a globe surface. The light ray intersects with the surface on entrance and exit. The lower panel shows a reconstruction of the fibre photoconductivity on the spherical surface, using electrical-current measurements obtained from the fibres, revealing the points of entrance and exit allowing the determination of the ray 3D trajectory. **c**, A fabric woven out of integrated photosensitive fibres, each externally surrounded by an omnidirectional reflector including a resonant microcavity (see Fig. 5). Such a fabric may deliver imaging and spectroscopic functionalities over a large area.

crystalline domains with superior electronic properties could be incorporated within fibre devices. These in turn may enable electronic junction structures (p-n, Schottky, and so on) for optoelectronic and logic operations. Many other characteristics

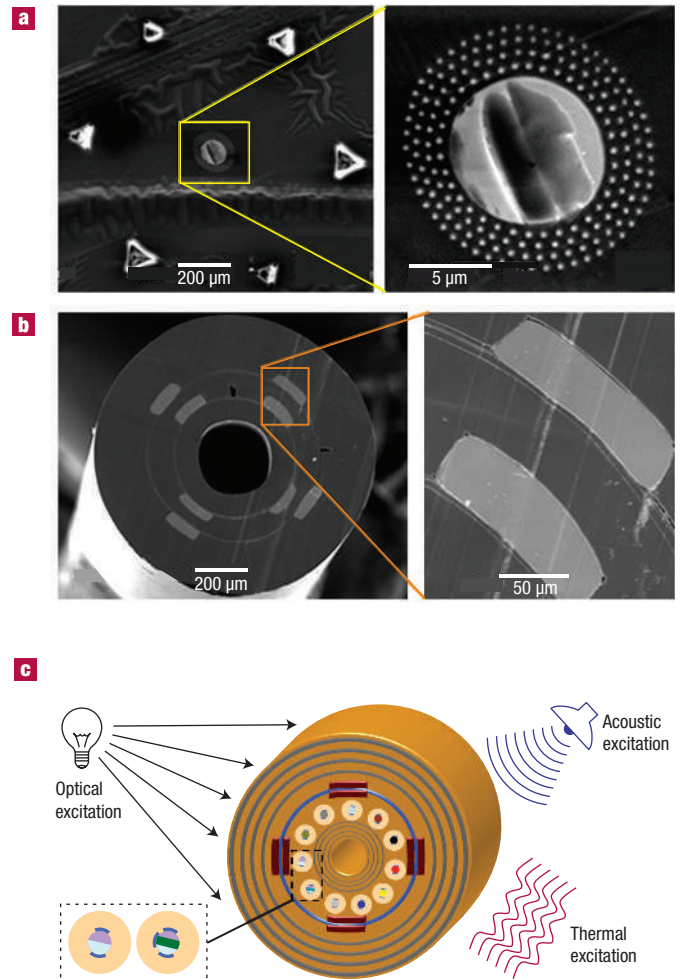


Figure 8 Fibre-device integrated bundles produced by stacking and redrawing. **a**, An array of chalcogenide-glass nanowires surrounding a solid-core of highly nonlinear chalcogenide glass. **b**, Two concentric thin-semiconductor-film devices integrated into the same fibre. **c**, Future vision of integrated fibre-device bundles. A single fibre consists of a hollow core lined with an omnidirectional reflector for optical-power transmission. The fibre is surrounded with another omnidirectional reflector, which may contain multiple cavities, for spectral filtering of externally incident radiation. The fibre contains thin-film semiconducting devices, and also multiple devices distributed over the cross-section, with each device sensitive to a different environmental parameter (light, heat, acoustic waves and so on). Logical operations may also be implemented with simple semiconductor junctions, two of which are shown in the inset.

make the glasses particularly useful. For example, As_2Se_3 in particular exhibits Kerr nonlinearity almost three orders of magnitude higher than silica glass^{71–75}. It is thus to be expected that nonlinear optical effects, such as supercontinuum generation^{76,77} and Raman amplification⁷⁸, founded on these multimaterial glass fibres will emerge. Other properties include high magneto-optic (Verdet) coefficients⁷⁹, amongst many others, readily suggesting a wide range of compact fibre-based devices. As the development of electronic functionality of these fibres continues, intriguing new devices lie ahead. The inclusion of metallic structures in these fibres enables static or time-varying electrical and magnetic fields to be set up. Hollow-core fibres have been used for particle and atom guiding by radiation pressure⁴⁶, and the close proximity of

controllable electric and magnetic fields enhances the capabilities of such systems, especially in biomedical applications where discrimination amongst particles and pathogens can now be extended by directly probing not only their optical but also their electric and/or magnetic response. This line of research could eventually lead to the development of a 'lab in a fibre', where several parallel or cascaded diagnostics may be applied to particles driven along the fibres. We envision the integration of many diverse fibre-based devices into a single fibre by stacking and redrawing (see Fig. 8). To date eight distinct functional devices have been incorporated into a single fibre structure. Fabrics that are woven either completely or partially from such integrated fibres can deliver a wide range of real-time, non-traditional functionalities over the full surface area of clothing, powered by electrical energy harvested from the ambient environment. The interplay between materials properties and structure integration in these fibres, alongside fabric-array construction, is just beginning, and promises to be an exciting field for fundamental and applied research. The further development of transistors and fibre-integrated logic devices would bring even more sophisticated functionalities and the prospect of truly multifunctional fabrics.

doi:10.1038/nmat1889

References

- Maurer, R. D. & Schultz, P. C. Fused silica optical waveguide. US patent 3,659,915 (1972).
- Keck, D. B., Maurer, R. D. & Schultz, P. C. On the ultimate lower limit of attenuation in glass optical waveguides. *Appl. Phys. Lett.* **22**, 307–309 (1973).
- Senior, J. M. *Optical Fiber Communications: Principles and Practice* (Prentice Hall, New Jersey, 1985).
- Agrawal, G. P. *Fiber-Optic Communication Systems* 3rd edn (Wiley-Interscience, New York, 2002).
- Marcuse, D. *Theory of Dielectric Optical Waveguides* (Academic, New York, 1974).
- Ramaswami, R. & Sivarajan, K. N. *Optical Networks: A Practical Perspective* (Morgan Kaufmann, San Francisco, 1998).
- Knight, J. C. et al. All-silica single-mode optical fiber with photonic crystal cladding. *Opt. Lett.* **21**, 1547–1549 (1996).
- Birks, T. A., Knight, J. C. & Russell, P. S. Endlessly single-mode photonic crystal fiber. *Opt. Lett.* **22**, 961–963 (1997).
- Cregan, R. F. et al. Single-mode photonic band gap guidance of light in air. *Science* **285**, 1537–1539 (1999).
- Yablonovitch, E. Inhibited spontaneous emission in solid-state physics and electronics. *Phys. Rev. Lett.* **58**, 2059–2062 (1987).
- John, S. Strong localization of photons in certain disordered dielectric superlattices. *Phys. Rev. Lett.* **58**, 2486–2489 (1987).
- Joannopoulos, J. D., Meade, R. D. & Winn, J. N. *Photonic Crystals: Molding the Flow of Light* (Princeton Univ. Press, New Jersey, 1995).
- Knight, J. C. Photonic crystal fibers. *Nature* **424**, 847–851 (2003).
- Russell, P. Photonic crystal fibers. *Science* **299**, 358–362 (2003).
- Nguyen, H. et al. A new slant on photonic crystal fibers. *Opt. Express* **12**, 1528–1539 (2004).
- Yeh, P., Yariv, A. & Marom, E. Theory of Bragg fiber. *J. Opt. Soc. Am.* **68**, 1196–1201 (1978).
- Winn, J. N. et al. Omnidirectional reflection from a one-dimensional photonic crystal. *Opt. Lett.* **23**, 1573–1575 (1998).
- Fink, Y. et al. A dielectric omnidirectional reflector. *Science* **282**, 1679–1682 (1998).
- Fink, Y. et al. Guiding optical light in air using an all-dielectric structure. *J. Lightwave Technol.* **17**, 2039–2041 (1999).
- Temelkuran, B. et al. Wavelength-scalable hollow optical fibres with large photonic bandgaps for CO₂ laser transmission. *Nature* **420**, 650–653 (2002).
- Hart, S. D. et al. External reflection from omnidirectional dielectric mirror fibers. *Science* **296**, 510–513 (2002).
- Benoit, G. et al. Static and dynamic properties of optical microcavities in photonic bandgap yarns. *Adv. Mater.* **15**, 2053–2056 (2003).
- Bayindir, M. et al. Metal-insulator-semiconductor optoelectronic fibres. *Nature* **431**, 826–829 (2004).
- Benoit, G. et al. Dynamic all-optical tuning of transverse resonant cavity modes in photonic bandgap fibres. *Opt. Lett.* **30**, 1620–1622 (2005).
- Shapira, O. et al. Surface-emitting fiber lasers. *Opt. Express* **14**, 3929–3935 (2006).
- Bayindir, M. et al. Fiber photodetectors codrawn from conducting, semiconducting and insulating materials. *Opt. Photon. News* **15**, 24 (2004).
- Bayindir, M. et al. Integrated fibres for self-monitored optical transport. *Nature Mater.* **4**, 820–825 (2005).
- Bayindir, M. et al. Thermal-sensing fiber devices by multimaterial codrawing. *Adv. Mater.* **18**, 845–849 (2006).
- Abouraddy, A. F. et al. Large-scale optical-field measurements with geometric fibre constructs. *Nature Mater.* **5**, 532–536 (2006).
- Rayleigh, L. On the stability of jets. *Proc. London. Math. Soc.* **10**, 4–13 (1878).
- Rayleigh, L. On the capillary phenomena of jets. *Proc. R. Soc. London* **29**, 71–97 (1879).
- Rayleigh, L. On the instability of a cylinder of viscous liquid under capillary force. *Phil. Mag.* **34**, 145–154 (1892).
- Tomotika, S. On the instability of a cylindrical thread of a viscous liquid surrounded by another viscous fluid. *Proc. R. Soc. London A* **150**, 322–337 (1935).
- Eggers, J. Nonlinear dynamics and breakup of free-surface flows. *Rev. Mod. Phys.* **69**, 865–929 (1997).
- Hilton, A. R. Optical properties of chalcogenide glasses. *J. Non-Cryst. Solids* **2**, 28–39 (1970).
- Sanghera, J. S. & Aggarwal, I. D. Active and passive chalcogenide glass optical fibers for IR applications: A review. *J. Non-Cryst. Solids* **257**, 6–16 (1999).
- Varshneya, A. K. *Fundamentals of Inorganic Glasses* (Academic, New York, 1994).
- Borisova, Z. U. *Glassy Semiconductors* (Plenum, New York, 1981).
- King, W. A., Clare, A. G. & Lacourse, W. C. Laboratory preparation of highly pure As₂Se₃ glass. *J. Non-Cryst. Solids* **181**, 231–237 (1995).
- Seddon, A. B. Chalcogenide glasses - A review of their preparation, properties and applications. *J. Non-Cryst. Solids* **184**, 44–50 (1995).
- Southworth, G. C. High frequency wave guides — general considerations and experimental results. *Bell System Tech. J.* **15**, 284–309 (1936).
- Warters, W. D. WT4 millimeter waveguide system - Introduction. *Bell System Tech. J.* **56**, 1825–1827 (1977).
- Alsberg, D. A., Bankert, J. C. & Hutchison, P. T. WT4-WT4a millimeter-wave transmission-system. *Bell System Tech. J.* **56**, 1829–1848 (1977).
- Mitra, P. P. & Stark, J. B. Nonlinear limits to the information capacity of optical fibre communications. *Nature* **411**, 1027–1030 (2001).
- Verdaasdonk, R. M. & van Swol, C. F. P. Laser light delivery systems for medical applications. *Phys. Med. Biol.* **42**, 869–894 (1997).
- Renn, M. J. et al. Laser-guided atoms in hollow-core optical fibers. *Phys. Rev. Lett.* **75**, 3253–3256 (1995).
- Constant, E. et al. Optimizing high harmonic generation in absorbing gases: Model and experiment. *Phys. Rev. Lett.* **82**, 1668–1671 (1999).
- Schnurer, M. et al. Guiding and high-harmonic generation of sub-10-fs pulses in hollow-core fibers at 10¹⁵ W/cm². *Appl. Phys. B* **67**, 263–266 (1998).
- Miyagi, M. & Kawakami, S. Design theory of dielectric-coated circular metallic waveguides for infrared transmission. *J. Lightwave Technol.* **2**, 116–126 (1984).
- Hongo, A. et al. Transmission of kilowatt-class CO₂-laser light through dielectric-coated metallic hollow wave-guides for material processing. *Appl. Opt.* **31**, 5114–5120 (1992).
- Miyagi, M. & Nishida, S. A proposal of low-loss leaky wave-guide for submillimeter waves transmission. *IEEE Trans. Microwave Theory.* **28**, 398–400 (1980).
- Desterke, C. M., Bassett, I. M. & Street, A. G. Differential losses in Bragg fibers. *J. Appl. Phys.* **76**, 680–688 (1994).
- Kuriki, K. et al. Hollow multilayer photonic bandgap fibers for NIR applications. *Opt. Express* **12**, 1510–1517 (2004).
- Harrington, J. A. A review of IR transmitting, hollow waveguides. *Fiber Integrated Opt.* **19**, 211–227 (2000).
- Dai, J. W. & Harrington, J. A. High-peak-power, pulsed CO₂ laser light delivery by hollow glass waveguides. *Appl. Opt.* **36**, 5072–5077 (1997).
- Strong, M. S. & Jako, G. J. Laser surgery in larynx: Early clinical experience with continuous CO₂-laser. *Ann. Oto. Rhinol. Larynx.* **81**, 791–798 (1972).
- Shapshay, S. M. & Beamis, J. F. Use of CO₂-laser. *Chest* **95**, 449–456 (1989).
- Anastassiou, C. et al. Fibers deliver CO₂ laser beams for medical applications. *Photon. Spectra* **38**, 108 (2004).
- Holsinger, F. C. et al. Use of the photonic band gap fiber assembly CO₂ laser system in head and neck surgical oncology. *Laryngoscope* **116**, 1288–1290 (2006).
- Devaiah, A. K. et al. Surgical utility of a new carbon dioxide laser fiber: Functional and histological study. *Laryngoscope* **115**, 1463–1468 (2005).
- Jacobson, A. S., Woo, P. & Shapshay, S. M. Emerging technology: Flexible CO₂ laser waveguide. *Otolaryng. Head Neck* **135**, 469–470 (2006).
- Pfeiffer, G., Paesler, M. A. & Agarwal, S. C. Reversible photodarkening of amorphous arsenic chalcogenides. *J. Non-Cryst. Solids* **130**, 111–143 (1991).
- Shimakawa, K., et al. A model for the photostructural changes in amorphous chalcogenides. *Phil. Mag. Lett.* **77**, 153–158 (1998).
- Ntziachristos, V., Bremer, C. & Weissleder, R. Fluorescence imaging with near-infrared light: new technological advances that enable in vivo molecular imaging. *Eur. Radiol.* **13**, 195–208 (2003).
- Koncar, V. Optical fiber fabric displays. *Opt. Photon. News* **16**, 40–44 (2005).
- Llyoyd, J. M. *Thermal Imaging Systems* (Plenum, New York, 1975).
- Dereniak, E. L. & Boreman, G. D. *Infrared Detectors and Systems* (Wiley, New York, 1996).
- Ahn, D. H. et al. A nonvolatile memory based on reversible phase changes between fcc and hcp. *IEEE Electron Dev. Lett.* **26**, 286–288 (2005).
- Liu, B. et al. Characteristics of chalcogenide nonvolatile memory nano-cell-element based on Sb₂Te₃ material. *Microelectron. Eng.* **82**, 168–174 (2005).
- Sun, Z. M., Zhou, J. & Ahuja, R. Structure of phase change materials for data storage. *Phys. Rev. Lett.* **96**, 055507 (2006).
- Lenz, G. et al. Large Kerr effect in bulk Se-based chalcogenide glasses. *Opt. Lett.* **25**, 254–256 (2000).
- Asobe, M. et al. 3rd-order nonlinear spectroscopy in As₂S₃ chalcogenide glass-fibers. *J. Appl. Phys.* **77**, 5518–5523 (1995).
- Spalter, S. et al. Strong self-phase modulation in planar chalcogenide glass waveguides. *Opt. Lett.* **27**, 363–365 (2002).
- Asobe, M. et al. laser-diode-driven ultrafast all-optical switching by using highly nonlinear chalcogenide glass-fiber. *Opt. Lett.* **18**, 1056–1058 (1993).
- Gopinath, J. T. et al. Third order nonlinearities in Ge-As-Se-based glasses for telecommunications applications. *J. Appl. Phys.* **96**, 6931–6933 (2004).
- Ranka, J. K., Windeler, R. S. & Stentz, A. J. Visible continuum generation in air-silica microstructure optical fibers with anomalous dispersion at 800 nm. *Opt. Lett.* **25**, 25–27 (2000).
- Birks, T. A., Wadsworth, W. J. & Russell, P. S. Supercontinuum generation in tapered fibers. *Opt. Lett.* **25**, 1415–1417 (2000).

78. Slusher, R. E. *et al.* Large Raman gain and nonlinear phase shifts in high-purity As₂Se₃ chalcogenide fibers. *J. Opt. Soc. Am. B* **21**, 1146–1155 (2004).
79. Ruan, Y. L. *et al.* Wavelength dispersion of Verdet constants in chalcogenide glasses for magneto-optical waveguide devices. *Opt. Comm.* **252**, 39–45 (2005).
80. Johnson, S. G. *et al.* Low-loss asymptotically single-mode propagation in large-core OmniGuide fibers. *Opt. Express* **9**, 748–779 (2001).
81. Ibanescu, M. *et al.* Analysis of mode structure in hollow dielectric waveguide fibers. *Phys. Rev. E* **67**, 046608 (2003).
82. Shapira, O. *et al.* Complete modal decomposition for optical waveguides. *Phys. Rev. Lett.* **94**, 143902 (2005).

Acknowledgements

The authors are indebted to John D. Joannopoulos for his support, dedication and vision without which the results reported would not have materialized. We thank S. Johnson, M. Soljagic, M. Ibanescu, J. Arnold, D. Deng, D. Saygin-Hinczewski and J-F. Viens. This work was supported by US Army ISN, ONR, AFRL, NSF, US DOE and DARPA. We also thank the RLE for its support. This work was also supported in part by the MRSEC Program of the National Science Foundation. Correspondence and requests for materials should be addressed to Y. F.

Competing financial interests

The authors declare no competing financial interests.